ChemComm

COMMUNICATION

View Article Online
View Journal | View Issue

Cite this: *Chem. Commun.*, 2014, **50**, 4000

Received 27th December 2013,
Accepted 25th February 2014

DOI: 10.1039/c3cc49796h

www.rsc.org/chemcomm

An electron transporting unit linked multifunctional Ir(III) complex: a promising strategy to improve the performance of solution-processed phosphorescent organic light-emitting diodes†

Thota Giridhar,[a] Chinnusamy Saravanan,[a] Woosum Cho,[a] Young Geun Park,[b] Jin Yong Lee*[b] and Sung-Ho Jin*[a]

An oxadiazole based electron transporting (ET) unit was glued to the heteroleptic Ir(III) complex (TPQIr-ET) and used as a dopant for phosphorescent organic light-emitting diodes (PhOLEDs). It shows superior device performance than the dopant without the ET unit (TPQIr) due to the balanced charge carrier injection by the ET unit.

The development of high performance solution-processed phosphorescent organic light-emitting diodes (PhOLEDs) has attracted significant research interest owing to their foreseeable impact in the field of inexpensive large area and flexible display devices.[1] PhOLEDs using Ir(III) complexes as emitters have drawn more attention due to their potential of 100% internal quantum efficiency *via* harvesting of both singlet and triplet excitons.[2] Among the phosphorescent emitters, homoleptic and heteroleptic cyclometalated Ir(III) complexes are still the most promising phosphors due to their relatively short triplet lifetimes, high quantum yields, and emission wavelength tunability from blue to deep-red.[3–5] Particularly, the color of the emitters can be tuned by the introduction of electron-donating or electron-accepting units and increasing or decreasing the extended π-conjugation in the ligands. In contrast, the performance of the particular emitter depends mainly on its interaction with the host materials, which are holes[6] or electrons[7] or a mixture of hole and electron transporting[8] or bipolar materials.[9] Generally, the similar structural features of the ligands of emitter and host materials facilitate charge injection and transporting ability of the resultant PhOLEDs. For example, Ir(III) complexes with carbazole based ligands as the dopant and CBP [4,4′-di(carbazole-9-yl)biphenyl] or PVK [poly-(*N*-vinylcarbazole)] as host materials enhance the hole injection and transport ability of the PhOLEDs.[10] Particularly, upon using either hole transporting or electron transporting (ET) single host materials, there has been a charge imbalance due to the existence of higher hole or electron mobility.[11] Alternatively, the mixed and/or bipolar host materials can provide a more balanced injection and transport of both the charge carriers due to the balance between the charges.[8,9] Thus, we glued the oxadiazole based ET unit to the ancillary ligand of heteroleptic Ir(III) complex *via* an ether linkage to analyze its effect on the device performance without changing the luminance maximum. Here, the ET unit may further improve the balance between the charges.

For this purpose, a thiophene–phenylquinoline (TPQ) based main ligand and picolinic acid with the oxadiazole based ET unit as an ancillary ligand for the heteroleptic Ir(III) complex, **TPQIr-ET**, were successfully designed and synthesized; for comparison, a similar Ir(III) complex without the ET group, **TPQIr**, was also synthesized. The structures of **TPQIr-ET** and **TPQIr** are shown in Scheme 1. The solution-processed deep-red PhOLEDs were fabricated using these Ir(III) complexes as dopants and tris(4-carbazoyl-9-ylphenyl)-amine (TCTA)/1,3,5-tri(1-phenyl-1*H*-benzo[*d*]imidazol-2-yl)phenyl (TPBi) or TCTA/1,3-bis(5-(4-*tert*-butylphenyl)-1,3,4-oxadiazol-2-yl)-benzene (OXD-7) as mixed-host materials with the configuration of ITO/PEDOT:PSS/TCTA:TPBi (1 : 1) or TCTA : OXD-7 (1 : 1):dopant/TmPyPB/LiF/Al. The poly(3,4-ethylenedioxythiophene):poly(styrene-sulfonate) (PEDOT:PSS) and 3,3′-[5′-[3-(3-pyridinyl)phenyl]-[1,1′:3′,1″-terphenyl]-3,3″-diyl]bispyridine (TmPyPB) were used as the hole transporting layer and the electron transporting layer, respectively. The devices based on **TPQIr-ET** show an EQE of 20.59%, which is the highest value reported to date for red PhOLEDs prepared using a solution-process (Table S2, ESI†). Additionally, we found that the **TPQIr-ET** shows 25% higher external quantum efficiency (EQE) than the **TPQIr** due to the balanced charge carrier injection by the ET group.

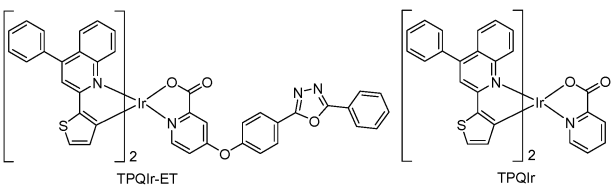

Scheme 1 Structure of **TPQIr-ET** and **TPQIr**.

[a] *Department of Chemistry Education, Graduate Department of Chemical Materials, and Institute for Plastic Information and Energy Materials, Pusan National University, Busan, 609-735, Republic of Korea. E-mail: shjin@pusan.ac.kr*

[b] *Department of Chemistry, Sungkyunkwan University, Suwon, 440-746, Republic of Korea. E-mail: jinylee@skku.edu*

† Electronic supplementary information (ESI) available: Experimental details, thermal stabilities and additional figures. See DOI: 10.1039/c3cc49796h

Both **TPQIr-ET** and **TPQIr** were synthesized in quantitative yields (Scheme S1, ESI†) and confirmed their structures by ^{1}H, ^{13}C NMR, elemental analysis, and high resolution mass spectroscopy (details are in the ESI†). They possess excellent solubility in common organic solvents, making them a suitable candidate for solution-processed PhOLEDs. Thermal gravimetric analysis under an N_2 atmosphere (Fig. S1, ESI†) reveals the onset decomposition temperatures to be 349 and 343 °C for **TPQIr-ET** and **TPQIr**, respectively, indicating their high thermal stability. Differential scanning calorimetry analysis (Fig. S2, ESI†) reveals the glass transition temperatures (T_g) to be 202 and 213 °C for **TPQIr-ET** and **TPQIr**, respectively, indicating their amorphous nature.

The UV-visible absorption and photoluminescence (PL) spectra of **TPQIr-ET** and **TPQIr** in methylene chloride (MC) solution at room temperature are shown in Fig. 1a. Both **TPQIr-ET** and **TPQIr** show two absorption bands: the broad bands between 550 and 450 nm corresponding to the admixture of singlet and triplet metal to ligand charge transfer (^{1}MLCT, ^{3}MLCT) transitions and the bands between 470 and 330 nm with a peak at 350 nm are attributed to the spin allowed π–π* transitions of the ligands. This indicates that the ET group in the **TPQIr-ET** does not show any significant effects on the ground state energy levels of Ir(III) complexes because the ET group is linked to the ancillary ligand by ether linkage, which prevents the extended π-conjugation between them. Additionally, the PL patterns of **TPQIr-ET** and **TPQIr** are also exactly similar with a maximum at 612 nm as shown in Fig. 1a and the quantum yield of 0.25 and 0.23, respectively. It also reveals that the ET group cannot induce any significant changes in the excited state of the Ir(III) complex, which leads to similar emission patterns and maxima.

In order to find highest occupied molecular orbital (HOMO) and lowest unoccupied molecular orbital (LUMO) energy levels, the cyclic voltammetry experiments were carried out for **TPQIr-ET** and **TPQIr** in MC solution (Fig. S3, ESI†). Both the Ir(III) complexes exhibited a well-defined reversible redox process. The HOMO energy levels were calculated from the onset of oxidation potentials and found to be −5.26 and −5.24 eV for **TPQIr-ET** and **TPQIr**, respectively. The LUMO levels were calculated from their HOMO levels and optical band gaps were determined from their absorption edges and found to be −3.07 and −3.08 eV for **TPQIr-ET** and **TPQIr**, respectively. As shown in Fig. 1b, the HOMO and LUMO energy levels of Ir(III) complexes are well matched with the adjacent layers of devices.

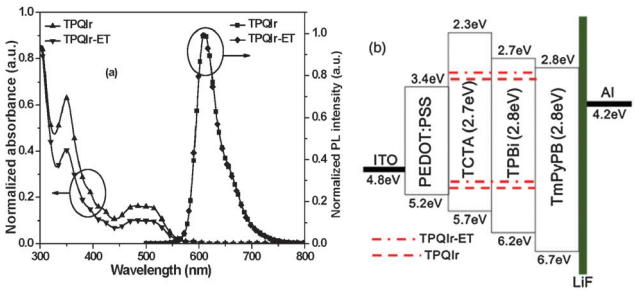

Fig. 1 (a) UV-visible and PL spectra of **TPQIr** and **TPQIr-ET** in MC and (b) energy level diagram of the materials.

Finally, from both optical and electrochemical properties, it was found that the introduction of the oxadiazole based ET group into **TPQIr-ET** does not have any significant influence on the energy levels of Ir(III) complexes. Density functional theory calculations were performed to gain an insight into the photophysical properties of both Ir(III) complexes. Becke's three parameter Lee–Yang–Parr exchange functional (B3LYP) and a suite of Gaussian 09 programs were employed.[12] Except for treating the Hay–Wadt effective core potential of a double zeta basis set (LANL2DZ) on Ir(III) metal, split valence 6-311+G** basis sets were used. The HOMOs are largely distributed over the Ir(III) metal and over one of the TPQ based main ligands while LUMOs are predominant on the ancillary ligand (Fig. S4, ESI†). These results show that the MLCT is likely to contribute to the transition properties. The calculated HOMO–LUMO energy levels of **TPQIr-ET** and **TPQIr** were 3.15 and 3.16 eV, which are almost similar to the experimentally determined energy levels of 3.09 and 3.12 eV, respectively. Particularly, the ET group in **TPQIr-ET** cannot involve in any of the energy levels.

To demonstrate the potential of the ET group in **TPQIr-ET** on the device performance, the solution-processed deep-red PhOLEDs (Fig. S5, ESI†) with various combinations of host and dopant materials (I, II, III, and IV), as shown in Table 1, were fabricated with the configuration of ITO/PEDOT:PSS/TCTA:TPBi or TCTA:OXD-7:dopant/TmPyPB/LiF/Al. Here, the emitting layer (EML) consists of a 1 : 1 ratio of TCTA and TPBi or OXD-7 with 8wt% of the **TPQIr-ET** or **TPQIr**. Fig. 2 shows the current density–voltage–luminance (*I*–*V*–*L*) and luminance efficiency–current density–power efficiency (LE–*I*–PE) curves of the all the devices and the data are summarized in Table 1.

Device I shows a current efficiency of 13.69 cd A^{-1} and an EQE of 15.28%, which are around 70% higher than that of device II, with a current efficiency of 5.09 cd A^{-1} and an EQE of 5.92%, respectively. It reveals that TPBi has a more balanced ET property with the hole transporting host TCTA than the OXD-7.

Table 1 Device characteristics of **TPQIr-ET** and **TPQIr** with various ratios of mixed host systems

Device	Host	Dopant	V_{on} [V]	EQE (%)	η_c [cd A^{-1}]	η_p [lm W^{-1}]	L_{max} [cd m^{-2}]
I	TCTA/TPBi	**TPQIr**	6.6	15.28	13.69	2.87	2013
II	TCTA/OXD-7	**TPQIr**	6.3	5.92	5.09	1.66	3013
III	TCTA/TPBi	**TPQIr-ET**	6.0	20.59	17.20	6.72	1334
IV	TCTC/OXD-7	**TPQIr-ET**	5.7	7.40	6.54	1.31	2661

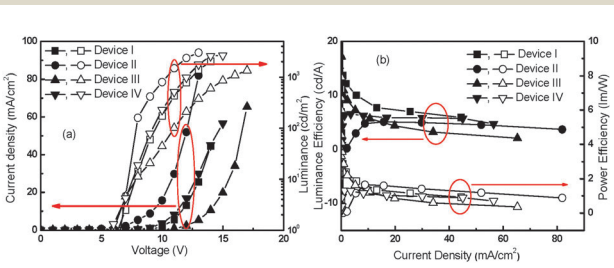

Fig. 2 (a) Current density–voltage–luminance (*I*–*V*–*L*) and (b) luminance efficiency–current density–power efficiency (LE–*I*–PE) curve of the devices based on **TPQIr-ET** and **TPQIr** dopants.

Similarly, device III shows a current efficiency of 17.20 cd A^{-1} and an EQE of 20.59%, which are around 60% higher than that of device IV, and a current efficiency of 7.40 cd A^{-1} and an EQE of 6.54%, respectively. Although both TPBi and OXD-7 have a good ET nature, the TPBi based devices show better device performance than that of OXD-7. This can be explained by the nature of the morphology engineering between TPBi and OXD-7 with TCTA (*vide infra*). Interestingly, the **TPQIr-ET** based devices show improved device performance compared to **TPQIr** due to the introduction of the ET group into the dopant materials, which is only 8 wt% of the dopant in EML and has a strong influence on balanced charge carrier injection. The hole transporting and ET properties of **TPQIr-ET** and **TPQIr** were further studied by fabricating hole and electron only devices (Fig. S6, ESI†). The mobility data are extracted in Table S1 (ESI†). It is obvious that the balance between hole and electron transport properties of **TPQIr-ET** is higher than that of **TPQIr** due to the presence of the ET group.

The morphology engineering between the host and the dopant materials can be analyzed using atomic force microscopy (AFM). AFM topographic images of 40 nm thick mixed-host TCTA : TPBi (1 : 1) and TCTA : OXD-7 (1 : 1) with 8 wt% of the **TPQIr** doped EML film are shown in Fig. 3a and b, respectively. Unexpectedly, the TCTA:TPBi based mixed-host system shows a higher root mean square surface roughness value (0.76 nm) than that of TCTA:OXD-7 (0.55 nm). This is due to the fact the TCTA and TPBi have a disk-like structure, which may be arranged in a columnar manner, but in the case of TCTA and OXD-7 based systems they may have an interdigitated future due to the rod-like nature of OXD-7. Thus, a balanced charge carrier injection is more feasible in the TCTA:TPBi system than in the TCTA:OXD-7 system. A similar trend has also been observed for **TPQIr-ET** (Fig. 3c and d). Interestingly, the introduction of the ET group into dopant materials improves the efficiency without engineering the morphology of the EML of the devices.

As shown in Fig. 4a, all the devices exhibited narrow deep-red electroluminescence (EL) spectra, which are similar to the PL spectra of the dopants. It suggests that the emission mainly originates from the triplet states of the Ir(III) complexes regardless of the nature of the host materials. As shown in Fig. 4b, devices I, II, III, and IV emit a deep-red light with the CIE coordinates of (0.671, 0.326), (0.671, 0.326), (0.673, 0.323), and (0.672, 0.325), respectively.

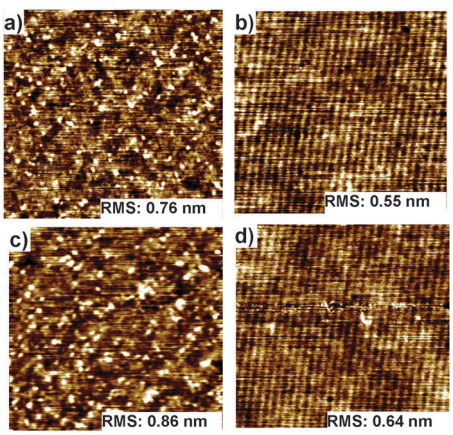

Fig. 3 AFM topographic images of (a) TCTA:TPBi:**TPQIr**, (b) TCTA:OXD-7:**TPQIr**, (c) TCTA:TPBi:**TPQIr-ET**, and (d) TCTA:OXD-7:**TPQIr-ET** based devices.

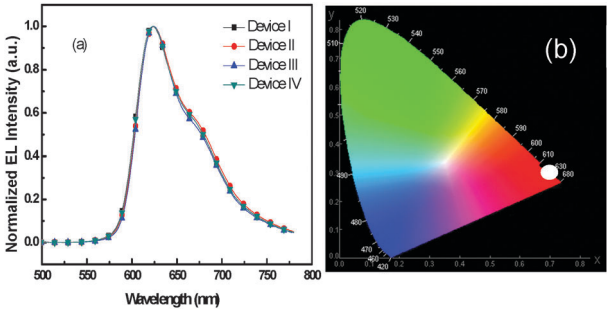

Fig. 4 (a) EL spectra and (b) CIE coordinate of devices I, II, III, and IV.

In summary, two heteroleptic Ir(III) complexes **TPQIr-ET** and **TPQIr** were designed, synthesized, and applied as a dopant for solution-processed deep-red PhOLEDs. Here, we introduced the ET group into the ancillary ligand of the dopant materials to improve the balanced charge carrier injection in the devices. As a result, **TPQIr-ET** shows an EQE value of 20.59%, which is 25% higher than that of **TPQIr**. This work provides the first successful example of the use of a dopant with the ET group in PhOLEDs to realize efficient device performance. This also opens up new perspectives in the designing of new phosphorescent emitters for efficient solution-processed PhOLEDs.

This work was supported by grant funding from the National Research Foundation of Korea (NRF) of the Ministry of Science, ICT & Future Planning (MSIP) of Korea (NRF-2011-0028320) and the Pioneer Research Center Program through the National Research Foundation of Korea funded by the Ministry of Science, ICT & Future Planning (MSIP) of Korea (NRF-2013M3C1A3065522). JYL acknowledges financial support from the NRF Grant (No. 2007-0054343) funded by the Korean Government.

Notes and references

1 J. H. Burroughes, D. D. C. Bradley, A. R. Brown, R. N. Marks, K. Mackay, R. H. Friend, P. L. Burn and A. B. Holmes, *Nature*, 1990, **347**, 539.
2 M. A. Baldo, D. F. O'Brien, Y. You, A. Shoustikov, S. Sibley, M. E. Thompson and S. R. Forrest, *Nature*, 1998, **395**, 151.
3 (*a*) D. H. Kim, N. S. Cho, H.-Y. Oh, J. H. Yang, W. S. Jeon, J. S. Park, M. C. Suh and J. H. Kwon, *Adv. Mater.*, 2011, **23**, 2721; (*b*) M. Song, J. S. Park, Y.-S. Gal, S. Kang, J. Y. Lee, J. W. Lee and S.-H. Jin, *J. Phys. Chem. C*, 2012, **116**, 7526.
4 B. Zhang, G. Tan, C.-S. Lam, B. Yao, C.-L. Ho, L. Liu, Z. Xie, W.-Y. Wong, J. Ding and S. L. Wang, *Adv. Mater.*, 2012, **24**, 1873.
5 D. H. Kim, N. S. Cho, H.-Y. Oh, J. H. Yang, W. S. Jeon, J. S. Park, M. C. Suh and J. H. Kwon, *Adv. Mater.*, 2011, **23**, 2721.
6 X. Gong, J. C. Ostrowski, G. C. Bazan, D. Moses and A. J. Heeger, *Appl. Phys. Lett.*, 2002, **81**, 3711.
7 G. Hughes and M. R. Bryce, *J. Mater. Chem.*, 2005, **15**, 94.
8 Y. Chen, J. Chen, Y. Zhao and D. Ma, *Appl. Phys. Lett.*, 2012, **100**, 213301.
9 A. Chaskar, H.-F. Chen and K.-T. Wong, *Adv. Mater.*, 2011, **23**, 3876.
10 C.-L. Ho, W.-Y. Wong, Q. Wang, D. Ma, L. Wang and Z. Lin, *Adv. Funct. Mater.*, 2008, **18**, 928.
11 C.-H. Hsiaoa, S.-W. Liua, C.-T. Chen and J.-H. Leea, *Org. Electron.*, 2010, **11**, 1500.
12 M. J. Frisch, *et al.* GAUSSIAN 03, Revision D.02, Gaussian Inc., Pittsburg, PA, 2006.

